Hindawi
International Journal of Chemical Engineering
Volume 2024, Article ID 5100871, 15 pages
https://doi.org/10.1155/2024/5100871

*Research Article*

# Research on the Aerodynamic Noise Characteristics of Heat Exchanger Tube Bundles Based on a Hybrid URANS-FWH Method

**Guofeng Huang,[1,2] Heng Wang,[2] Sheng Tian,[1,2] and Wei Tan[1,2]**

[1]*School of Chemical Engineering and Technology, Tianjin University, Tianjin, China*
[2]*Zhejiang Institute of Tianjin University, Ningbo, Zhejiang, China*

Correspondence should be addressed to Wei Tan; wtan@tju.edu.cn

Received 23 November 2023; Revised 2 January 2024; Accepted 8 January 2024; Published 31 January 2024

Academic Editor: Junwu Wang



This paper examines the aerodynamic noise characteristics of heat exchanger tube bundles, with the objective of exploring the frequency and directional features of noise under nonacoustic resonance conditions, to provide assistance in determining acoustic resonance. To predict the flow-induced noise of tube bundles, this study employs a hybrid URANS-FWH method. The transition SST model of URANS is used to accurately simulate the turbulent flow field and obtain precise statistical data on turbulence. The FWH equation is utilized to predict and evaluate the intensity and spectral characteristics of the tube bundle noise. The research findings indicate that the noise generated by the heat exchanger tube bundle is affected by pressure pulsations resulting from vortex motion in the deeper regions of the tube bundles. Notably, within specific frequency ranges, the noise intensity experiences a significant enhancement, potentially triggering complex modes of acoustic resonance. This resonance phenomenon poses safety concerns for equipment and threatens the wellbeing of personnel. Consequently, this study provides a solid theoretical foundation for predicting and controlling noise in heat exchanger tube bundles, offering valuable guidance for practical applications.

## 1. Introduction

Shell-and-tube heat exchangers are crucial equipment in industrial production systems, serving the purpose of heat transfer. With their simple structure and mature technology, they are extensively utilized in various fields such as chemical engineering, nuclear power, metallurgy, and pharmaceuticals. A multitude of heat transfer tubes contained within the heat exchanger constitute the primary components responsible for heat exchange, thereby directly influencing the performance and lifespan of the heat exchanger.

Fluid-induced vibrations are a critical factor contributing to the failure of heat transfer tubes. This phenomenon is commonly attributed to four mechanisms: turbulent buffeting, vortex shedding excitation, fluid-elastic instability, and acoustic resonance [1]. It is important to note that acoustic resonance specifically occurs in heat exchangers where the medium on the shell side is a gas. When the fluid strikes the tube bundle, it creates periodic flow structures within the bundle. If the frequency of the noise approaches and meets certain conditions related to the acoustic modes of the shell, a positive feedback loop can be established between the flow field and the acoustic field, leading to the occurrence of acoustic resonance [2–4]. The significant noise generated during acoustic resonance poses a threat to the safety of surrounding equipment and the health of personnel.

The investigation of sound generated by vortex shedding in tube bundles within heat exchangers under nonacoustic resonance conditions has received limited attention, despite its potential to assess whether the frequency conditions for acoustic resonance are met. Currently, few studies have been conducted on this subject matter. Heat transfer tubes can be simplified as cylindrical structures, and their flow-induced

noise issues can be classified as cylinder wake noise. Zhou [5] conducted aerodynamic noise simulations on a tube bundle model comprising nine tubes and summarized the influence of the pitch-to-diameter ratio on the frequency and intensity of the noise. Tang et al. [6] simplified finned tubes as circular tubes and investigated the vortex shedding noise of tube arrays, thereby achieving noise source identification in waste heat boilers.

In the aerospace field, landing gear noise can also be simplified as a cylinder wake noise problem, and extensive research has been conducted in this area. The National Aeronautics and Space Administration (NASA) has conducted high-precision noise experiments on tandem circular cylinders in acoustic wind tunnels [7], providing fundamental models for the development of numerical simulation techniques. Liu [8] employed the Lighthill analogy method to predict the noise of tandem circular cylinders, achieving good agreement with experimental results. In addition, it was found that the flow field at this Reynolds number exhibits complex three-dimensional characteristics, making it challenging to accurately capture the flow field features through two-dimensional simulations. Spalart et al. [9] investigated the influence of integral surface selection on the prediction of noise in tandem circular cylinders using the FWH equation. They discovered that employing permeable integral surfaces yielded better results than using solid surfaces, although the reliability of this method still requires further verification over time. In order to investigate the flow dynamics around two tandem circular cylinders at both subcritical and supercritical Reynolds numbers, Hu et al. [10] conducted an extensive three-dimensional numerical simulation of tandem cylinders. This study revealed distinct phenomena associated with vortex shedding, shear layer reattachment, and hydrodynamic forces, all of which were influenced by the spacing ratio (L/D) between the cylinders. Chen et al. [11] simulated the noise of tandem cylinders using an improved delayed detached eddy simulation model combined with acoustic perturbation, obtaining results that closely matched experimental data. They also validated the applicability of modal decomposition techniques for identifying characteristic frequencies in the flow field.

Flow-induced noise is a common issue in many application scenarios, and there have been numerous numerical simulation efforts dedicated to noise prediction [12–14]. Chode et al. [15] explore the aerodynamic noise generated by a standard squareback body with inclined side-view mirrors, employing a hybrid computational aeroacoustic method. The findings highlight that the absence of side-view mirrors reduces overall noise, attributing the A-pillar as a significant contributor. Varying mirror inclination angles not only impact the drag coefficient nonlinearly but also influence noise levels. Yangzhou et al. [16] investigate the aeroacoustic sources of a two-bladed propeller in an aerofoil wake using large eddy simulation and FWH equation. A novel near-field aeroacoustic source analysis based on the acoustic analogy is introduced, identifying various sources and correlating them with flow features, propeller surfaces, and noise spectra.

This study focuses on investigating the phenomenon of abnormal acoustic resonance that occurs in practical engineering applications. In preliminary work [17], the vibration characteristics and acoustic modes of the heat exchanger were determined. The findings from that research are briefly summarized in Section 3. In this paper, a two-dimensional model will be utilized in conjunction with a hybrid URANS-FWH method to assess the aerodynamic noise characteristics within the tube bundles more comprehensively. First, the validity of the two-dimensional model will be verified. Subsequently, a computational model for the aerodynamic noise of the tube bundles in the heat exchanger will be established to investigate the flow field and acoustic field. Finally, the results obtained from the calculation, incorporating the vibration characteristics and acoustic modes of the heat exchanger, will be utilized to explain the mechanism behind the occurrence of abnormal acoustic resonance in the heat exchanger.

## 2. Numerical Method

*2.1. Modeling of the Flow Field.* This study utilizes the finite volume method to solve the two-dimensional unsteady Reynolds-averaged Navier–Stokes (URANS) equations for flow at subcritical Reynolds numbers. The transition SST model is employed due to its excellent predictive accuracy. The model incorporates the intermittency factor $\gamma$ and the transport equations for the momentum thickness Reynolds number, as shown in the following equations:

$$\frac{\partial(\rho\gamma)}{\partial t}+\frac{\partial\left(\rho U_j\gamma\right)}{\partial x_j}=P_{\gamma1}-E_{\gamma1}+P_{\gamma2}-E_{\gamma2}+\frac{\partial}{\partial x_j}\left[\left(\mu+\frac{\mu_t}{\sigma_\gamma}\right)\frac{\partial\gamma}{\partial x_j}\right], \tag{1}$$

$$\frac{\partial(\rho\mathrm{Re}_{\theta t})}{\partial t}+\frac{\partial\left(\rho U_j\mathrm{Re}_{\theta t}\right)}{\partial x_j}=P_{\theta t}+\frac{\partial}{\partial x_j}\left[\sigma_{\theta t}(\mu+\mu_t)\frac{\partial\mathrm{Re}_{\theta t}}{\partial x_j}\right]. \tag{2}$$

In the equations, $P_{\gamma1}$ and $E_{\gamma1}$ represent the transition source terms, $P_{\gamma2}$ and $E_{\gamma2}$ represent the retransition source terms, $P_{\theta t}$ is the source term related to the momentum thickness Reynolds number $\mathrm{Re}_{\theta t}$, and $\sigma_{\theta t}$ is a constant in the calculation of the momentum thickness Reynolds number. More detailed information about this model can be found in [18].

The pressure fluctuations on the tube wall are primarily manifested as lift forces, which can be characterized by the lift coefficient. The definition of the lift coefficient is as follows:

$$C_L=\frac{L}{1/2\rho U^2D}, \tag{3}$$

where $L$ is the lift force, $\rho$ is the density of the fluid, $U$ is the velocity, and $D$ is the diameter of the tube.

This paper adopts the vorticity formulation to describe the vortical structures in the flow field, where vorticity is defined as the curl of the velocity vector in the $Z$-direction. The definition of vorticity is as follows:

$$Z \text{ vorticity} = \frac{\partial V_y}{\partial x} - \frac{\partial V_x}{\partial y}. \quad (4)$$

*2.2. Modeling of the Aerodynamic Noise.* The calculation of noise in this paper is conducted using the FWH (Ffowcs Williams and Hawkings) equation, which belongs to the acoustic analogy method. Compared to direct numerical methods and hybrid methods, this approach offers significant advantages in terms of computational resources and time efficiency. The FWH equation can be expressed in the following form [19]:

$$\frac{1}{a_0^2}\frac{\partial^2 p'}{\partial t^2} - \nabla^2 p' = \frac{\partial^2}{\partial x_i \partial x_j}\left\{T_{ij}H(f)\right\} - \frac{\partial}{\partial x_i}\left\{\left[P_{ij}n_j + \rho u_i(u_n - v_n)\right]\delta(f)\right\} + \frac{\partial}{\partial t}\left\{\left[P_0 v_n + \rho(u_n - v_n)\right]\delta(f)\right\}, \quad (5)$$

where $u_i$ and $v_i$ are the fluid velocity component and the surface velocity component in the $x_i$ direction, $u_n$ and $v_n$ are the fluid velocity component and the surface velocity component normal to the surface, $\delta(f)$ is the Dirac delta function, $H(f)$ is the Heaviside function, and $p'$ is the sound pressure at the far field ($p' = p - p_0$).

On the right-hand side of the equation, the three terms correspond to the monopole, dipole, and quadrupole sound sources, respectively. In cases where the Mach number is low and the wall is stationary, the dominant contribution to the sound field arises from the dipole sound source generated by the wall pressure fluctuations. Therefore, in this paper, the cylindrical wall is chosen as the integration surface, and the monopole and quadrupole sound sources are neglected.

## 3. Vibration Testing and Acoustic Modal Analysis

*3.1. Vibration Testing.* The collection of vibration signals was performed using a 1A342E triaxial accelerometer and a DH5920 signal acquisition system. During the pretesting phase, it was observed that the vibrations on the connected pipelines were significantly weaker than on the main body of the heat exchanger. Therefore, formal testing was conducted exclusively on the shell of the heat exchanger. Considering the overall on-site conditions, the measurement points were ultimately set at the inlet and outlet platforms of the shell side and tube side. The basic structure of the heat exchanger and the arrangement of measurement points are shown in Figure 1. The test results revealed the presence of vibrations in various parts of the heat exchanger, albeit with differences in vibration intensity. In the region of mild vibration, there was no significant difference observed among the three directions of vibration. However, in the region of severe vibration, the radial vibration was stronger, with the root mean square amplitude of radial vibration acceleration being 2 to 5 times greater than that of axial or tangential vibration acceleration.

The signals from measurement points within the same testing area exhibit similar characteristics. Here, we present the spectra of representative measurement points in Figure 2. The vibration signals are concentrated within a narrow low-frequency range, with multiple peaks observed in the frequency bands centered around 100 Hz, 128 Hz, and 145 Hz. Higher frequency signals have significantly weaker intensity, almost vanishing. In the region of relatively lower vibration intensity, there is no significant difference in the proportion of frequencies. However, on the shell side outlet platform where vibration intensity is higher, the 128 Hz component dominates completely, with peak amplitudes of 7.8 m/s$^2$ (radial), 1.8 m/s$^2$ (axial), and 1.3 m/s$^2$ (tangential). This indicates that 128 Hz is likely the primary characteristic frequency of the vibration excitation. Such tonal characteristics align with the "pure tone noise" typically associated with acoustic resonance. Based on the design conditions, the natural frequency of the tubes is 79 Hz, which significantly differs from 128 Hz. This suggests that the vibration and noise are not caused by local tube bundle flow-induced instability but rather by acoustic resonance.

*3.2. Acoustic Modal Analysis.* To investigate the cause of acoustic resonance and gain a deeper understanding, the finite element method can be utilized to calculate the acoustic cavity mode specifically within shell side of the shell outlet platform. Due to the presence of the tube bundle within the shell cavity, where the wavelength of sound waves is significantly larger than the gaps between the tubes, sound waves primarily propagate through diffraction from one side to the other. This phenomenon effectively increases the actual distance traveled by the sound waves. Consequently, it is reasonable to consider a reduced effective sound velocity within the tube bundle region when computing the acoustic modes. In this study, the method proposed by Kunihiko [20] was adopted to calculate the equivalent sound velocity:

$$c = \sqrt{\kappa \frac{p}{\rho}},$$
$$c_e = \frac{c}{\sqrt{1 + a\sigma}}\left(\text{where } a = \frac{10}{3}\sigma + \frac{1}{3}\right), \quad (6)$$

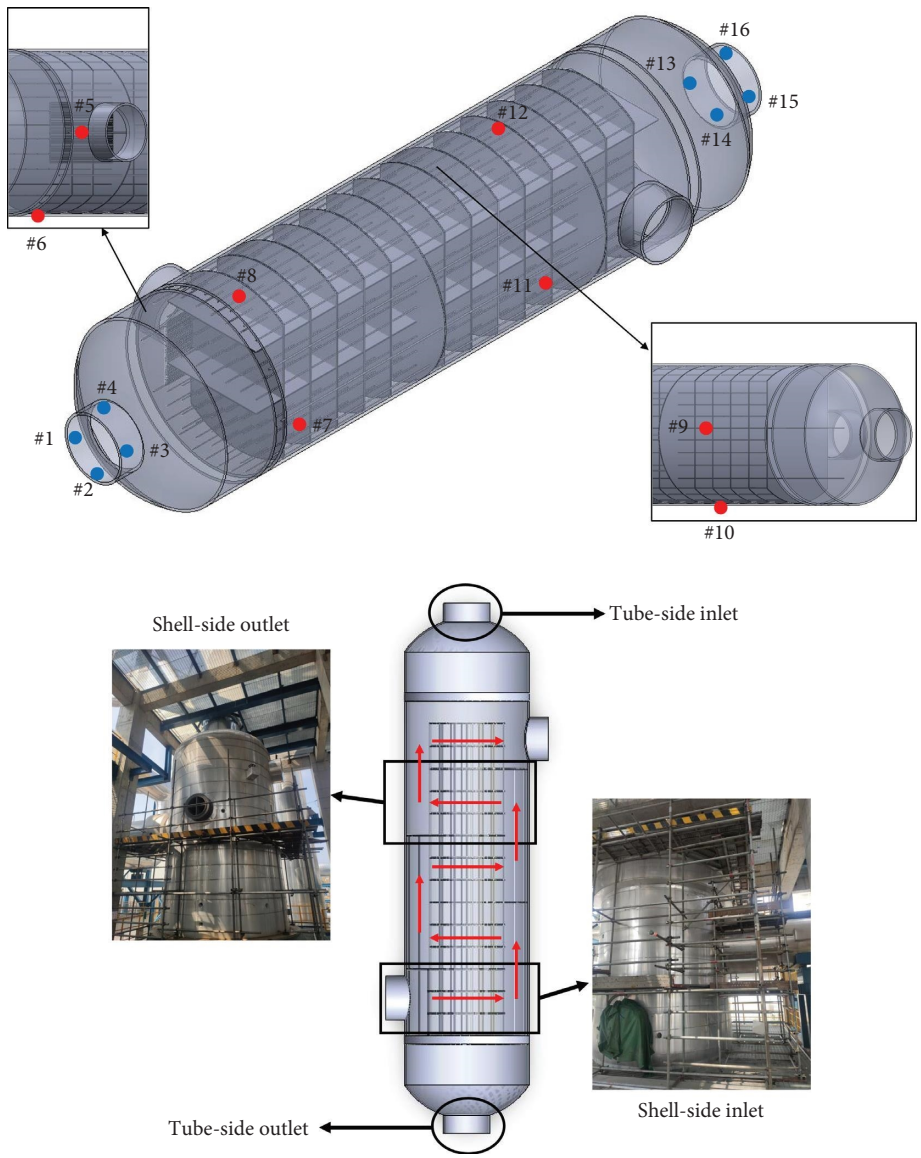


Figure 1: Configuration of vibration measurement locations.

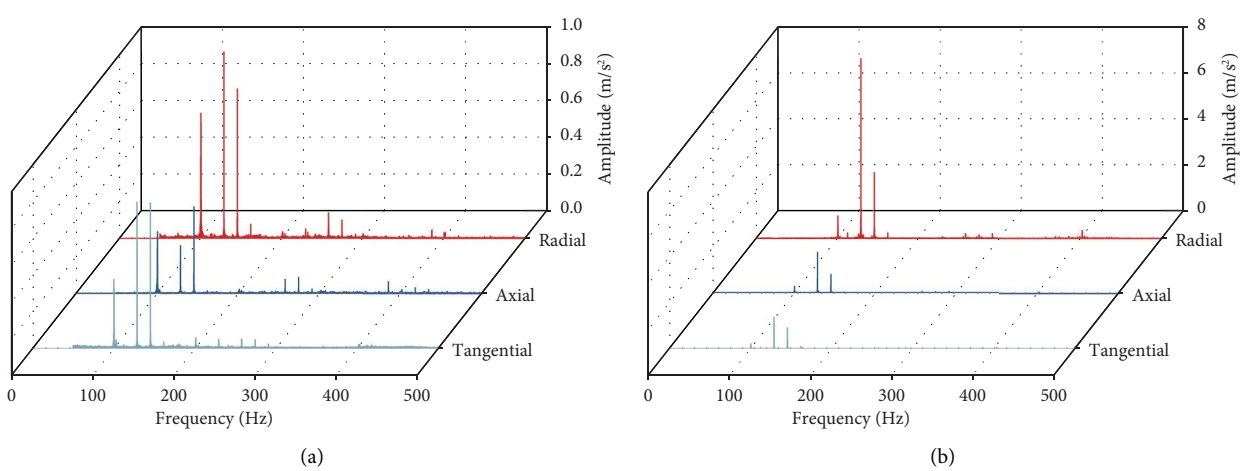


Figure 2: Typical measurement point spectrum signal. (a) Point #8. (b) Point #11.

where $\kappa$ represents the adiabatic coefficient of the medium, which is determined as 1.3, $p$ is the absolute operating pressure, $\sigma$ signifies the denseness of the tube bundle, which can be calculated based on the specific arrangement form and yields a value of 0.45 in this particular case, and $a$ is associated with $\sigma$. Upon performing the calculations, the sound velocity is determined to be 382.16 m/s, while the equivalent sound velocity is found to be 281.96 m/s.

The computed results of the acoustic modes are presented in Figure 3. Based on the direction of the acoustic modes, they can be classified into transverse modes (perpendicular to the flow direction and tube direction), longitudinal modes (parallel to the flow direction), and axial modes (parallel to the tube direction). Modes 1, 2, and 3 in the figure correspond to the first-order transverse acoustic modes of the three chambers after the addition of longitudinal baffles, which are the primary modes considered in the resonance analysis. Among them, Mode 2 at 103.03 Hz is close to the measured signal at 100 Hz, but it significantly deviates from the dominant characteristic frequency of 128 Hz.

Modes 4 and 5 represent the coupled modes of the wider two chambers in both transverse and longitudinal directions. These modes closely match the measured signals and are likely the modes excited in the resonance of this heat exchanger. Further investigations are required to examine the phenomenon of vortex shedding in the tube bundle region and the noise characteristics induced by fluid flow through the tube bundle in order to provide a more conclusive determination.

## 4. Simulation of the Tube Bundle Aerodynamic Noise

In general, studies on aerodynamic noise often employ methods such as DNS (direct numerical simulation) and LES (large eddy simulation). These methods offer high resolution in resolving the flow field and effectively capture turbulent fluctuations, making them well-suited for noise prediction. However, the Reynolds numbers of the flow in the shell side of heat exchangers typically fall within the subcritical range ($10^4$~$10^5$), where the flow exhibits significant three-dimensional effects. Considering the presence of numerous tube bundles in the shell side, conducting three-dimensional simulations using these methods would require significant computational resources, which is often impractical. Therefore, numerical simulations often simplify the flow to a two-dimensional representation.

However, a two-dimensional simplification implies the neglect of the third dimension of vortex motion, meaning the lack of spanwise effects. This leads to deviations between the results obtained from DNS, LES, and the actual situation, making them unsuitable for the present study. The URANS (unsteady Reynolds-Averaged Navier–Stokes) models retain the large-scale information of the flow field and accurately capture the dominant fluctuating components of the flow during calculations. When applied to two-dimensional flow field calculations, URANS models show good agreement with experimental results. Among these models, the SST (shear stress transport) model exhibits high accuracy in predicting boundary layer separation and has been widely used in past studies on cylinder flow. The transition SST model, derived from the SST model, can provide reasonably accurate predictions of the flow characteristics in the near-wall region of cylinders [21].

It must be highlighted that the application of 2D-URANS simulations has inherent limitations in predictive accuracy when addressing the separated reverse flow problem within high Reynolds number flows. This deficiency persists even within the framework of three-dimensional flow simulations that meticulously account for turbulent anisotropy [22, 23]. In the context of a multiple-cylinder array in a heat exchanger, the flow separation on the cylinder surface is notably influenced by the arrangement of surrounding cylinders, involving interference from adjacent cylinders' structures and separated flows. In the case of adopting this method, the presence of discrepancies is foreseeable. While various approaches have been explored in the existing literature for noise prediction in this context, the application of 2D-URANS models remains rare. Therefore, it is essential to assess the applicability of this method to determine whether the associated errors are acceptable.

The inline arrangement is one of the basic configurations of heat transfer tubes. Before conducting calculations for the aerodynamic noise of tube bundles, this study will establish a test model based on the experimental setup of a tandem cylinder aerodynamic noise experiment conducted by NASA's wind tunnel [8]. The test model will be subjected to calculations using two different models: the $k$-$\omega$ SST (shear stress transport) model and the transition SST model. The results will be compared with experimental data to validate the predictive capability of the methods employed in this study for flow-induced noise in such flow configurations.

*4.1. Validation of Numerical Methods.* The computational domain was established based on the experimental setup [8], as shown in Figure 4. Two cylinders with a diameter of 57.15 mm were arranged in tandem in the wind tunnel, aligned with the direction of the wind flow. The distance between the two cylinders was 3.7 D. The upstream length was 5 D, and the downstream length was 15 D. The width of the computational domain was 10 D.

At the inlet, a velocity inlet boundary condition was applied, and at the outlet, a pressure outlet boundary condition was used. The upper and lower boundaries were treated as symmetry boundaries, and the cylinder walls were modeled as nonslip walls. The flow medium was air, and the Reynolds number based on the cylinder diameter (Re) was $1.66 * 10^5$. The noise-receiving points were set according to the experimental configuration, and their coordinates were as follows: Receiver A (−8.33 D, 27.815 D), Receiver B (9.11 D, 32.49 D), and Receiver C (26.55 D, 27.815 D).

An O-type structured grid was used for mesh generation, and the meshing results are shown in Figure 5. A refined boundary layer mesh was applied along the cylinder walls, with a first-layer height of approximately $10^{-3}$ D, satisfying the condition $y^+ < 1$. The boundary layer growth rate was set

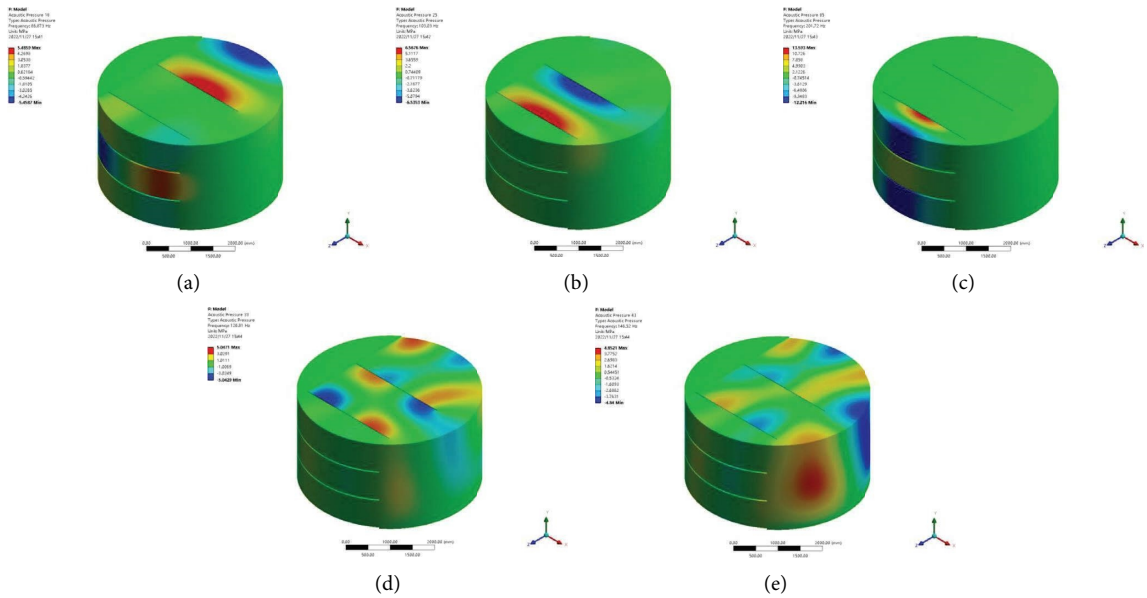


Figure 3: Results of acoustic modal analysis. (a) Mode 1 at 86.87 Hz. (b) Mode 2 at 103.03 Hz. (c) Mode 3 at 201.72 Hz. (d) Mode 4 at 126.82 Hz. (e) Mode 5 at 146.52 Hz.

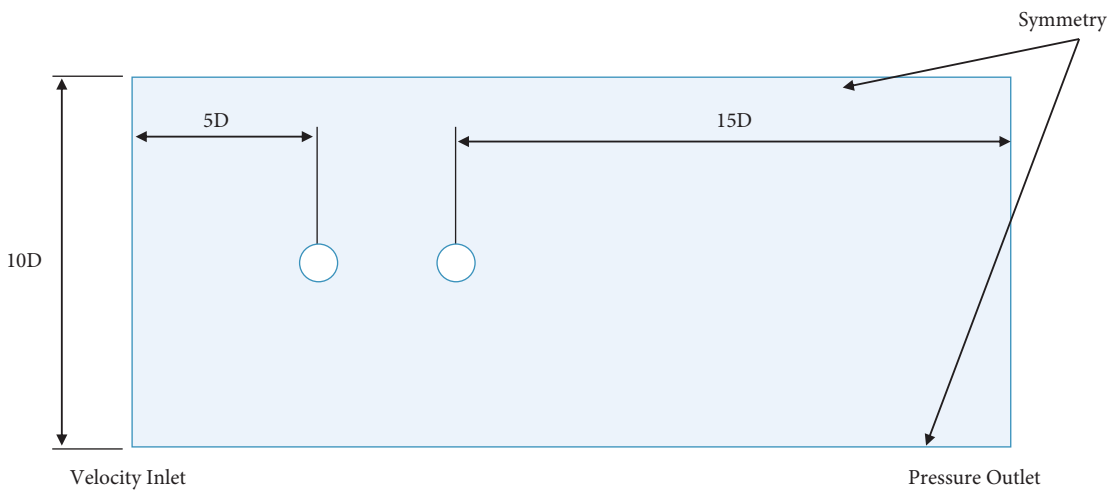


Figure 4: Calculation domain for the tandem cylinder model.

to 1.05. The total number of generated grids was 166,568. To capture the vortex behavior near the cylinder walls and the gap between the cylinders, a small time step of $2 * 10^{-5}$ s was used for the computation [24].

In Table 1, the average and root-mean-square (RMS) values of lift and drag coefficients on the surfaces of both upstream and downstream cylinders are presented, utilizing the transition SST model with varying grid resolutions. The comparative analysis of experimental results indicates that, under the current grid configuration, the results obtained using the transition SST model are in good agreement with the experimental data. The surface pressure coefficient distribution on the cylinder in the time-averaged flow field is depicted in Figure 6. Both models exhibit similar trends in the surface pressure coefficient distribution compared to the experimental data. However, there are some disparities between the models in certain regions of the upstream cylinder surface. The $k$-$\omega$ SST model provides a better prediction of the negative pressure region, while the transition SST model performs more accurately in predicting the separation region and the location of the lowest pressure coefficient. On the downstream cylinder surface, both models deviate significantly from the experimental results, a departure from findings in other study [26]. This discrepancy arises from the three-dimensional effects of the vortices generated by the cylinder flow at this Reynolds number. The wake vortex produced by the upstream cylinder directly interacts with the downstream cylinder, leading to the formation of numerous broken vortices. The URANS model, which considers primarily two-dimensional

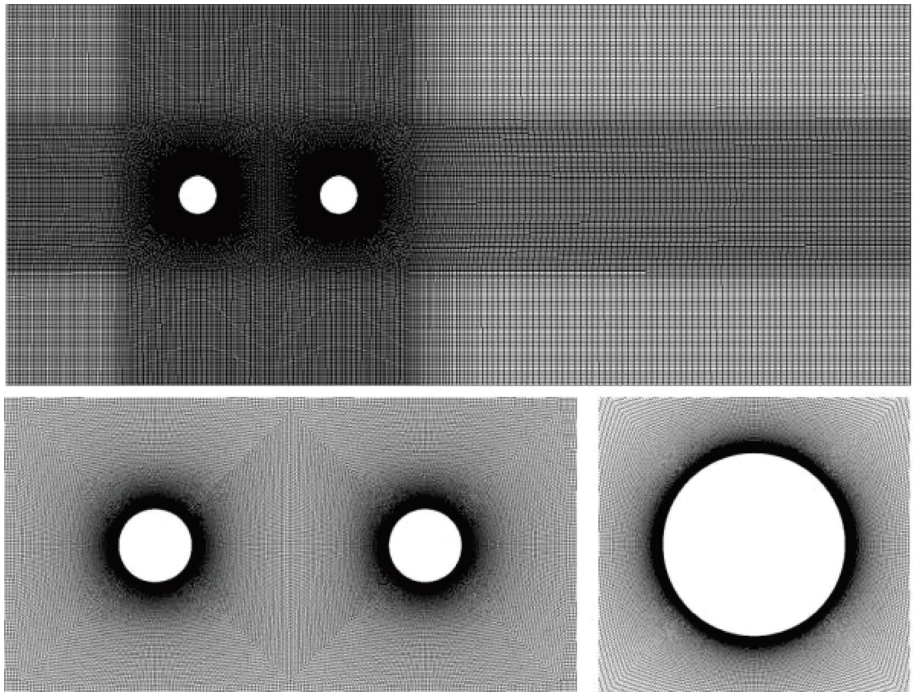

Figure 5: Schematic diagram of mesh division for the tandem cylinder model.

Table 1: Grid independence validation for inline cylinders.

| Models | Nodes | $C_{D\,\mathrm{up}}$ | $C_{L\,\mathrm{rms,up}}$ | $C_{D\,\mathrm{down}}$ | $C_{L\,\mathrm{rms,down}}$ |
|---|---|---|---|---|---|
| Case 1 | 121,464 | 0.569 | 0.174 | 0.338 | 0.503 |
| Case 2 | 166,568 | 0.584 | 0.185 | 0.341 | 0.515 |
| Case 3 | 238,596 | 0.587 | 0.191 | 0.346 | 0.517 |
| Experiment [25] | — | 0.59–0.63 | — | 0.29–0.31 | — |

fluctuations in the flow field, cannot capture the full three-dimensional structure of these vortices. Consequently, it struggles to predict the impact of these broken vortices on vortex shedding and the resulting distribution of surface pressure on the downstream cylinder, resulting in deviations from the experimental data. It is important to acknowledge that such errors are inherent in 2 D simulations. Taking all these factors into consideration, the transition SST model has been chosen for the present study.

The noise signals at the receiver points are extracted from the flow field using the FWH equation. Before applying the fast Fourier transform (FFT) to extract frequency-domain information, a Hanning window function is applied to the data windows of three receivers, all with equal length. This same processing is extended to the noise signals from tube bundles in the subsequent analysis. Figure 7 illustrates the sound pressure level signals at each receiver point, while Table 2 presents the calculated peak frequencies and corresponding sound pressure levels. A two-dimensional model was utilized in this study, and the sound pressure level was found to be dependent on the source correlation length, which was determined through experimental measurements. A source correlation length of 2.72 D = 155.45 mm is reported in [26]. It can be observed that the low-frequency noise is well predicted, with a peak frequency difference of 2 Hz and a maximum sound pressure level difference of 2.4 dB. The calculated frequencies and sound pressure levels align closely with the experimental results. The peak frequency of the noise corresponds to the shedding frequency of vortices in the flow field, representing the primary source of noise in the flow around a cylinder. However, at higher harmonic frequencies, the sound pressure predictions deviate significantly, with the sound pressure levels at each receiver point being considerably higher than in the experimental results, indicating an overestimation of the sound pressure levels at harmonic frequencies.

During acoustic experiments conducted by NASA, a transition strip was installed on the surface of the cylinder to induce vortex shedding that differs from the shedding behavior of a smooth cylinder. However, in both two-dimensional and three-dimensional models, the cylinder surface was assumed to be smooth, without considering the presence of the transition strip. Therefore, while the peak frequencies obtained from the two-dimensional model in this study are slightly higher and closer to the experimental results than those from the three-dimensional model, it does not necessarily imply that the two-dimensional results are more accurate. It is merely a coincidence. The two-

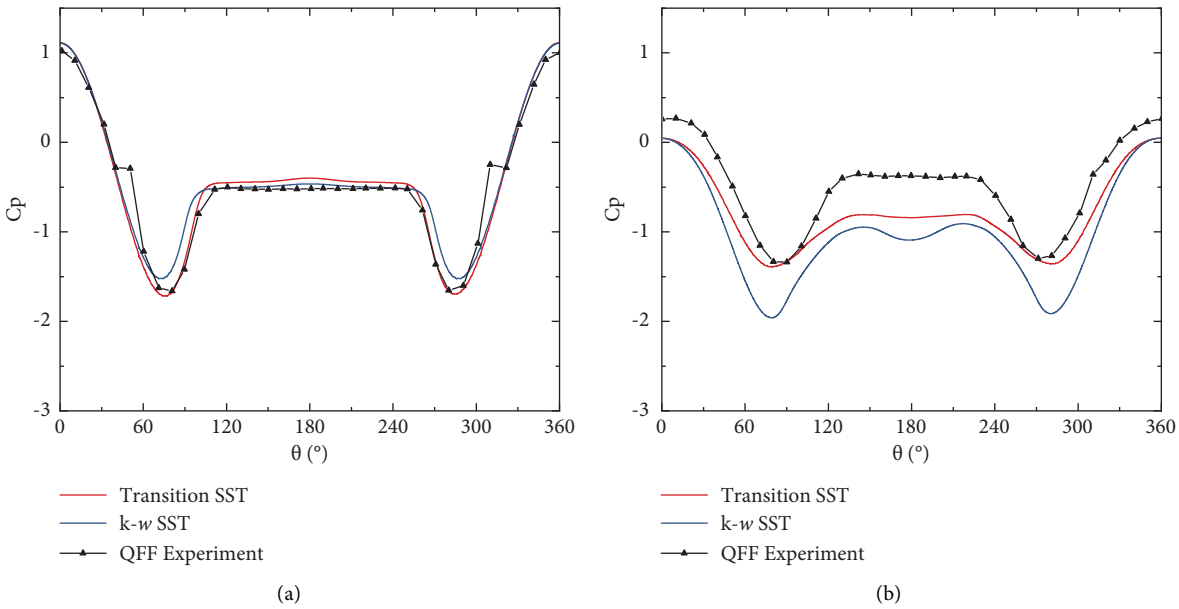


Figure 6: Distribution of surface pressure coefficient on the cylinder in time-averaged flow field. (a) Upstream cylinder surface pressure coefficient distribution. (b) Downstream cylinder surface pressure coefficient distribution.

Table 2: Results for the peak frequency and sound pressure level (SPL) at the receivers.

| Receiver points | 2D simulation | | 3D simulation [9] | | Experimental results [8] | |
|---|---|---|---|---|---|---|
| | Peak frequency (Hz) | SPL (dB) | Peak frequency (Hz) | SPL (dB) | Peak frequency (Hz) | SPL (dB) |
| Receiver A | 180 | 91.7 | 172 | 92.1 | 178 | 94.1 |
| Receiver B | 180 | 93.3 | 172 | 92.4 | 178 | 95.6 |
| Receiver C | 180 | 90.3 | 172 | 91.3 | 178 | 92.7 |

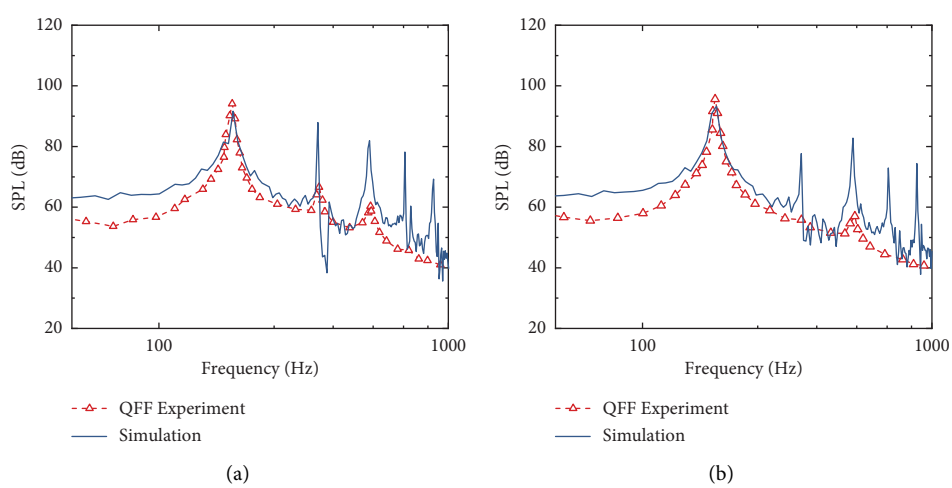


Figure 7: Continued.

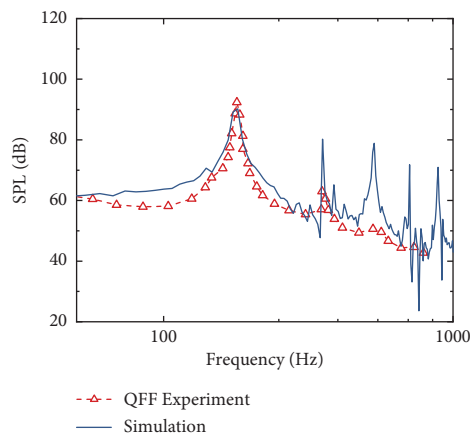


(c)

Figure 7: Spectrum plot of sound pressure level (SPL) signal at the receiver point. (a) Receiver A. (b) Receiver B. (c) Receiver C.

dimensional model employed the URANS model, which tends to overestimate the Reynolds stresses in the wake, leading to an overestimation of the shedding frequency and causing the inaccurate prediction of noise at high harmonic frequencies. The transient results obtained from this model exhibit more pronounced tonal characteristics [18].

In comparison to the three-dimensional model, the adoption of a two-dimensional computation offers significant advantages in terms of reduced grid cell count, resulting in notable time and resource savings. This approach proves to be cost-effective. Although simplifying the flow field to two dimensions leads to the loss of certain flow field information and introduces deviations in predicting the pressure distribution on the cylinder surface and sound pressure at harmonic frequencies, it does not compromise the accurate prediction of the dominant frequency components of flow field fluctuations. Therefore, this method exhibits a high level of reliability in predicting noise at characteristic frequencies.

*4.2. Modeling of the Tube Bundle Aerodynamic Noise.* The current limitations in computational resources make it challenging to perform calculations on heat exchanger tube models at their actual scale. Therefore, research on the aerodynamic noise response characteristics requires the reduction of tube bundle sizes. Currently, there is limited numerical simulation research available on the aerodynamic noise of heat exchanger tube bundles. In low Mach number flows, the predominant source of noise arises from pressure fluctuations generated by vortices on the tube bundle walls, acting as dipole sound sources. Through the literature review, it has been observed that the flow conditions near the edges of the tube bundle, several rows upstream and downstream, differ significantly from those in the deeper regions of the bundle. A relatively stable flow state is achieved only after several rows of tubes have been traversed. In the deeper regions of the tube bundle, each tube wall exhibits similar characteristic pressure fluctuations. Therefore, studying vortex shedding within tube bundles requires a minimum tube bundle size. Tang et al. [27] recommend a minimum model size of 8 rows and 11 columns for tube bundles. In this study, a tube bundle model consisting of 11 rows and 13 columns is employed, as depicted in Figure 8, surpassing the minimum size required for investigating vortex shedding in the deeper regions of the bundle. According to the actual heat exchanger configuration, the tube bundle model utilizes a rotated square arrangement. The outer diameter of the tube is 19 mm, and the pitch-to-diameter ratio is 1.33. The entrance length is 10 d, the exit length is 15 d, and mesh refinement is applied within the 5 d long wake region. The coordinate origin is set at the center of the central tube, and two noise receiver points, Receiver 1 (0, 20 d) and Receiver 2 (−20 d, 0), are positioned in the lift and drag directions, respectively.

The actual tube bundles in heat exchangers are of considerable size, and their aerodynamic noise is predominantly influenced by the internal tubes rather than the tubes at the edge of the bundle. If all tubes were considered as sound sources in a simplified model, the impact of the edge tubes would be exaggerated compared to the real scenario. Assuming that there is a disparity in the flow conditions between the surrounding flow field of the six rows of tubes at the bundle's edge and the internal tubes (although different studies may slightly vary in the number of rows), it is possible that nearly half of the noise contribution originates from these edge tubes, significantly affecting the analysis of the noise from the internal tubes. Conversely, selecting a single tube as the research object makes it challenging to comprehensively capture the stochastic nature of vortex motion deep within the bundle, thus hindering the acquisition of statistically significant aerodynamic noise characteristics of the tube bundle. Therefore, in this study, the central tube and its eight neighboring tubes were chosen as the sound sources to investigate the aerodynamic noise characteristics of the tube bundle in heat exchangers.

For descriptive purposes, let us label the central tube as "tc" and starting from the first tube adjacent to its left side, we will proceed clockwise, labeling them as "t1" through

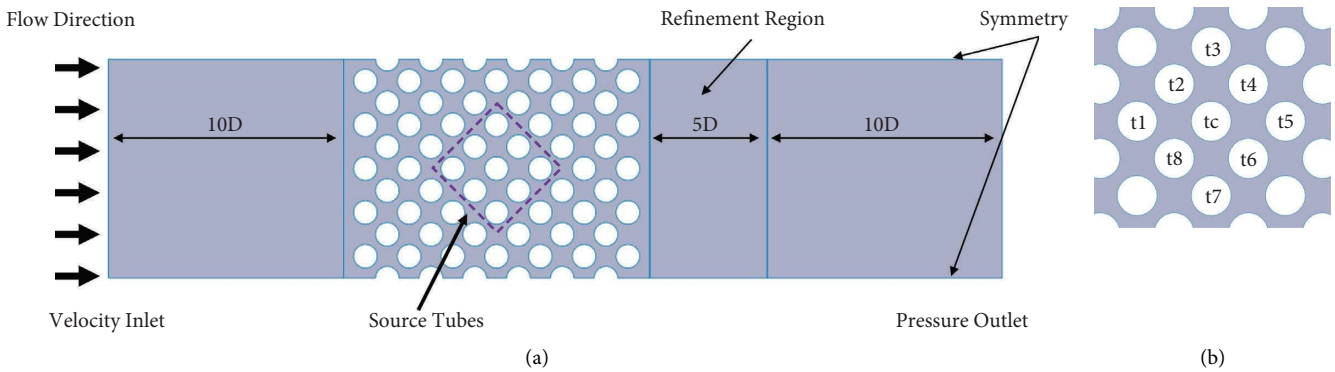


Figure 8: Schematic diagram of tube bundle aerodynamic noise calculation model. (a) Geometric model for tube bundle aerodynamic noise calculation. (b) Source zone.

"t8." The fluid flows into the tube bundle from the left side and exits from the right side after passing through the bundle. The boundary conditions at the inlet and outlet are set as the velocity inlet and pressure outlet, respectively. The upper and lower walls are treated as symmetry planes to allow for tangential fluid motion and minimize the impact of the boundaries on the flow field within the central tube bundle.

The coupling of pressure and velocity is achieved using the SIMPLE (semi-implicit method for pressure-linked equations) method. Second-order upwind schemes are employed for spatial discretization of pressure, momentum, and turbulence, while the Green–Gauss cell-based method is used for gradient calculations. Time advancement is carried out using a second-order finite difference method. Prior to the transient calculations, a steady-state simulation is performed, with the steady-state results serving as the initial values for the transient simulation. To ensure a relatively stable flow field, the first 0.5 seconds of the transient simulation are dedicated to achieving this state, corresponding to approximately 60 vortex shedding cycles. Subsequently, the flow field information is recorded and utilized for subsequent analysis for a duration of 1 second, representing approximately 120 vortex shedding cycles. During the computations, the lift coefficients of the central tube and the surrounding eight tubes are monitored. Following the completion of the calculations, fast Fourier transform (FFT) is applied to obtain frequency spectra for further analysis. To capture the intricate motion of vortices within the tube bundle, a time step size of $5 * 10^{-5}$ s is utilized. Each vortex shedding cycle encompasses approximately 160 computational steps. The residual criterion is set to $10^{-5}$, and a maximum of 50 iterations per time step are performed to ensure convergence.

The tube bundle region exhibits a complex geometric structure, which is divided using a triangular mesh. The inlet and outlet sections are discretized using a quadrilateral mesh. Grid refinement is applied to the wake region. The tube walls are represented by a finely resolved boundary layer mesh, consisting of 25 layers with a first grid layer height of approximately $10^{-4}$ d, ensuring that $y^+ < 1$. The growth rate is set to 1.2. The grid is shown in Figure 9. To ensure grid independence, three sets of grids are prepared: Case 1 with 450,000 cells, Case 2 with 630,000 cells, and Case 3 with 800,000 cells. The lift coefficient spectra for the central tube bundle obtained from these grid sets are shown in Figure 10. For a more comprehensive analysis of the flow field and noise characteristics, the results from Case 2 have been chosen as the most representative.

*4.3. Results and Discussion.* The velocity and vorticity distributions within the tube bundle region, as obtained from the calculations, are presented in Figure 11. The flow field in the deep region of the tube bundle exhibits a highly intricate structure. On the one hand, as the fluid traverses the tube bundle, the variation in the flow area leads to the formation of high-speed fluid jets within the gaps between the tubes. On the other hand, a substantial number of vortices are generated and shed behind the tubes in the deep region of the tube bundle. These vortices attach themselves to the downstream tube walls. Notably, there are instances where vortices of the opposite direction shed from adjacent tube walls, resulting in the formation of high-speed jet pairs that influence the fluid dynamics.

It is important to note that the present study employs the URANS model, which retains primarily the dominant vortex structures, while finer details are not captured. This approach is justified as the primary objective of this study is to investigate the predominant modes of vortex motion in the deep region of the tube bundle and the major frequency characteristics of the noise, rather than providing a comprehensive prediction of the flow field and noise. The vorticity distribution reveals that the intensity of vortices in the deep region of the tube bundle surpasses that in the wake region behind the tube bundle. These vortices induce periodic variations in fluid pressure along the tube walls, resulting in the generation of sound waves. Under specific conditions, these sound waves may be reflected by the walls, potentially leading to acoustic resonance.

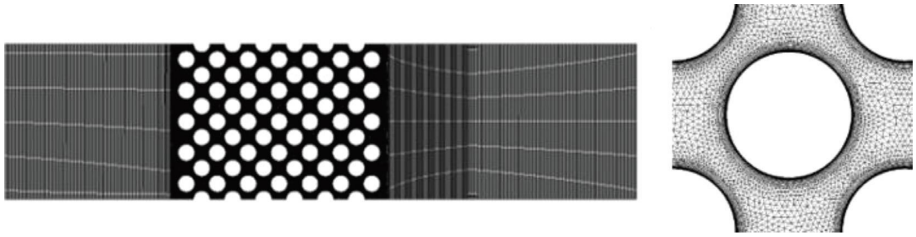

Figure 9: Grid overview for tube bundle aerodynamic noise calculation model.

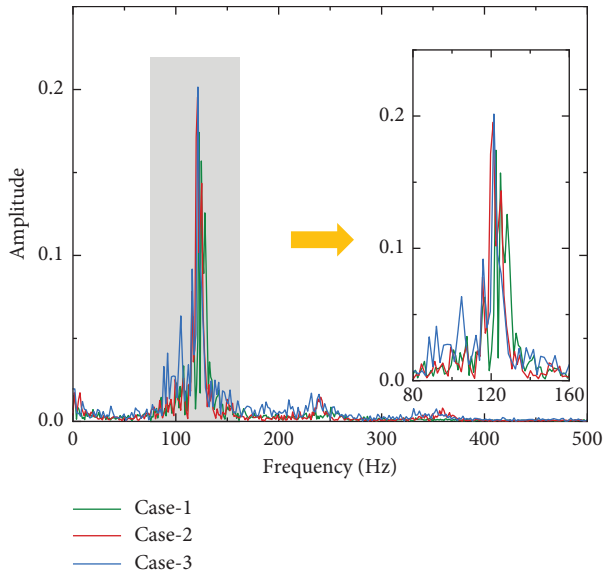


Figure 10: Grid independence verification.

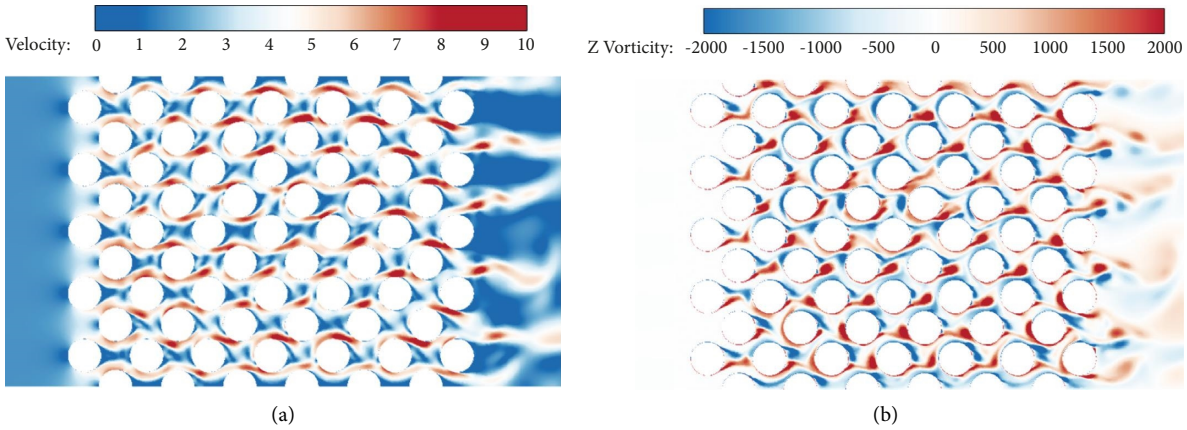


Figure 11: The distribution of velocity and vorticity in tube bundles. (a) Velocity contour. (b) Vorticity contour.

The shedding behavior of vortices in the deep region of the tube bundle is influenced by multiple factors. When vortices detach from the upstream tube wall and reach the downstream tube wall, they reattach and generate pressure fluctuations that affect the shedding process of subsequent vortices. In addition, interactions between shed vortices can alter their motion characteristics. In the downstream direction, there are three neighboring tubes. The shedding motion of vortices can be categorized into two modes based on their attachment patterns, which are shown in Figure 12. In one mode, vortices travel along the flow direction and reattach to the immediate downstream tube wall. In the other mode, vortices attach to the wall surfaces of the adjacent upper and lower tubes. However, the presence of high-speed flow in the gap between tubes and the influence of vortices shedding from neighboring tube walls limit the

occurrence of vortices attaching to the upper and lower adjacent tubes. Even if such attachment occurs, the effects are mitigated by the high-speed flow, making them secondary in terms of their impact on wall pressure fluctuations. These two modes of motion can coexist within the development process of a single vortex, where the vortex separates into two parts during the shedding process: one part attaches to the immediate downstream tube wall, while the other part attaches to the upper and lower adjacent tube walls. In general, vortex motion exhibits significant randomness, making it challenging to predict accurately.

The lift coefficient variations of the tubes were recorded over a certain time period to analyze the impact of random vortex motion on wall pressure fluctuations. The resulting lift coefficient spectrum for the source tubes is depicted in Figure 13. Despite the unpredictable fluid motion, the wall pressure fluctuations at the source tube walls exhibit similar frequency characteristics. Notably, the lift coefficients consistently peak around 121 Hz, indicating that the flow field around the selected source tubes has reached a "relatively stable" state, allowing for the investigation of aerodynamic noise in the deeper region of the tube bundle. In addition, secondary peaks are observed within the frequency band centered on the main peak of the lift coefficient. These secondary peaks can be attributed to the combined effects of vortex shedding caused by the impingement of the fluid on the tubes and the pulsating pressure resulting from the random attachment behavior of vortices. These findings highlight the inherent complexity of lift coefficient fluctuations in the tube bundle and underscore the significance of considering both vortex shedding and random attachment behavior to comprehensively understand the characteristics of aerodynamic noise.

To further ascertain the propagation characteristics of noise in different directions, multiple receiving points were strategically placed along the circumference at a distance of 20 d from the reference point to capture the noise signals. These signals were then subjected to FFT processing and transformed into sound pressure levels, allowing us to obtain the directional features of the noise, as illustrated in Figure 14. From the analysis of the figure, it is evident that the noise exhibits dipole characteristics. Regardless of the overall sound pressure level or the sound pressure level at the peak frequency, the noise levels are consistently higher in the cross-flow direction than in the downstream direction. This phenomenon can be attributed to the dominant presence of pressure fluctuations along the direction of wall lift in the flow field of the bundle region. Consequently, the resulting noise is stronger in the cross-flow direction than in the drag direction. This observation aligns with previous studies on flow-induced vibration in bundles, which have demonstrated that the amplitude of cross-flow vibration is typically greater than that of the downstream vibration. Moreover, the cross-flow direction is more susceptible to instability. The dipole characteristics exhibited by the noise are likely an essential factor contributing to the excitation of lateral acoustic modes rather than longitudinal modes when acoustic resonance occurs in heat exchangers.

To further analyze the phenomenon of the inconsistent intensity of bundle noise in different directions at the lift frequency, we conducted FFT processing and analyzed the sound pressure signals from Receiver 1 positioned at 0° and Receiver 2 positioned at 90°. The sound pressure level spectra for these two points are depicted in Figure 15. From the graph, it is evident that both receiving points exhibit peak values at the same frequency. The first peak frequency corresponds to the primary fluctuation frequency of the lift coefficient, which is associated with vortex shedding. The higher frequency range shows the harmonics of the first peak frequency. At the peak frequency, Receiver 1, located in the cross-flow direction, registers stronger noise intensity at 105.67 dB, whereas Receiver 2, positioned in the downstream direction, experiences a lower noise level at 91.62 dB. The noise level in the downstream direction is approximately 13.2% lower than that in the cross-flow direction.

Moreover, it is noteworthy that some numerical artifacts manifest in the high-frequency segment of the results. While the frequency increases, the difference in the sound pressure level at the peak frequencies between the two receiving points diminishes. They exhibit similar amplitudes at the first three harmonics before the lift frequency. However, beyond the frequency range of approximately 700 Hz, the disparity between the two signals becomes more prominent. After 1000 Hz, there is an upward trend observed in the noise from Receiver 2. It is important to acknowledge that this pattern does not accurately reflect the actual scenario. As mentioned earlier, the URANS model overlooks small vortex structures that contribute to high-frequency components in the flow field. It tends to overestimate harmonics, leading to a deviation in predicting the high-frequency range. The correction method for the high-frequency component of noise requires further investigation, which beyond the scope of the present study. In this study, the emphasis was primarily placed on the noise prediction results at the fundamental frequency.

In the studied heat exchanger, the actual vibration frequency of 128 Hz and the coupled mode Mode 4 at 126.82 Hz shown in Figure 3, along with the characteristic frequency of 121 Hz for the aerodynamic noise of the bundle, are highly similar. This indicates that the cause of abnormal acoustic resonance in this heat exchanger can be attributed to the primarily excited coupled mode Mode 4, with Mode 2 and Mode 5 playing a secondary role. The excitation of this coupled mode has rarely been reported in the past, and the longitudinal baffles only provide suppression for the transverse modes, not the longitudinal mode. Therefore, even with the presence of acoustic vibration isolation panels, the heat exchanger still experienced acoustic resonance. Although the dipole characteristics of the aerodynamic noise in the bundle make the transverse acoustic modes more prone to excitation, in the reported case, the dominance of coupled modes in both the transverse and longitudinal directions during acoustic resonance suggests that even the relatively smaller downstream noise can potentially trigger acoustic resonance and cannot be suppressed by transverse baffles. In future revisions of standards, it may be necessary to consider such scenarios to avoid their occurrence during the design phase.

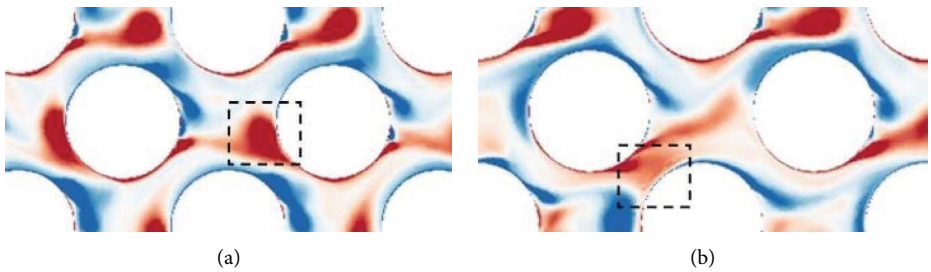


Figure 12: Main motion modes of vortices in tube bundles. (a) Attaching to the downstream tube. (b) Attaching to the upper and lower adjacent tubes.

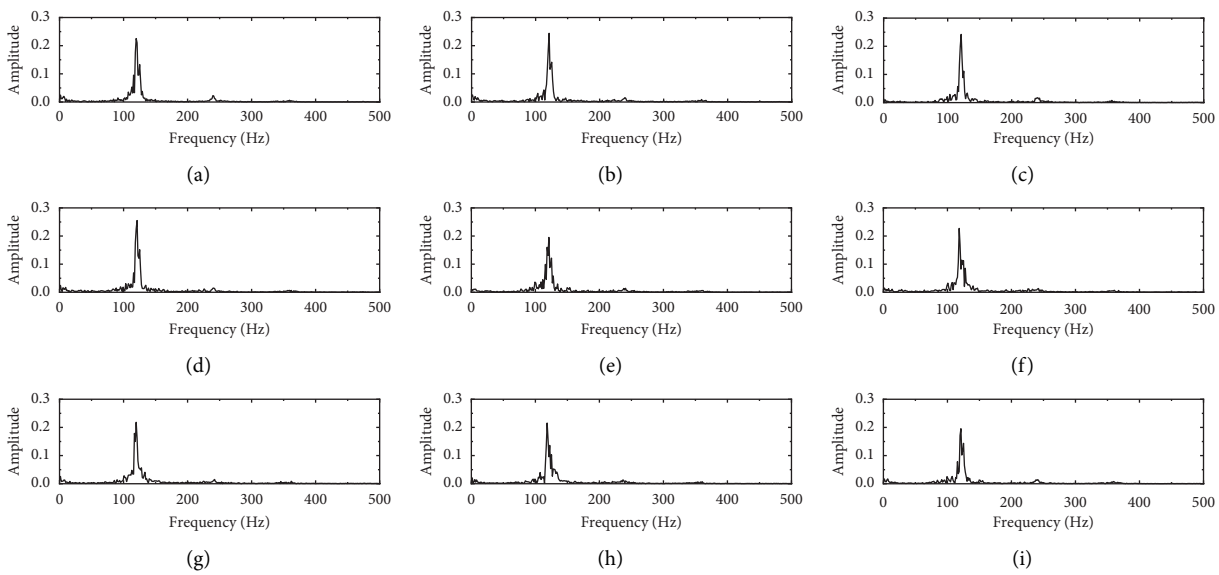


Figure 13: Spectrum of lift coefficient for source tubes. (a) t1. (b) t2. (c) t3. (d) t4. (e) t5. (f) t6. (g) t7. (h) t8. (i) tc.

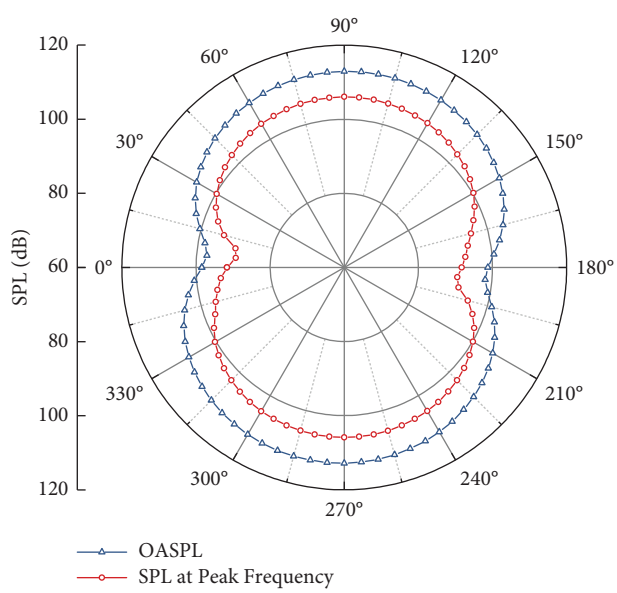


Figure 14: Sound pressure level (dB) directivity plot.

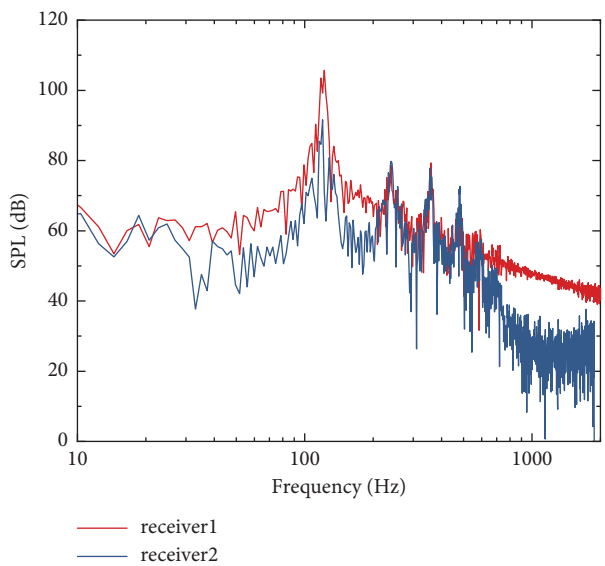


Figure 15: Sound pressure level spectrum at receivers.

## 5. Conclusion

In the preliminary work, experimental testing and acoustic mode calculations have already been conducted to investigate abnormal acoustic resonance in the heat exchanger. First, the reliability of the two-dimensional model with the hybrid URANS-FWH method for aerodynamic noise calculations was verified. Subsequently, a dedicated calculation model for bundle aerodynamic noise was developed. The investigation focused on the characteristics of the tube bundles' aerodynamic noise in the heat exchanger, aiming to determine the underlying causes of acoustic resonance. The following are the main findings and conclusions of the study:

(1) The study utilized a model identical to NASA's tandem cylinder experiment and employed a hybrid method of the URANS model and FWH equation for calculations. The predictions of the peak frequency and sound pressure level closely matched the experimental results, demonstrating good agreement. However, there was a discrepancy in predicting high-frequency noise, with an overestimation of amplitudes at harmonic frequencies. Nevertheless, when investigating the dominant frequency of the flow field, this methodology offers a reasonable level of reliability and cost-effectiveness.

(2) In the deep region of the tube array, a significant number of vortices detach from the tube walls, exhibiting random motion that is challenging to predict. These vortices' shedding and attachment behavior on the tube surface lead to pressure fluctuations and the generation of aerodynamic noise. The peak frequency of the noise occurs at the lift frequency and is primarily observed in the lift direction, exhibiting prominent dipole characteristics. At a distance of 20 d from the central tube bundle, the transverse noise level measures 105.67 dB, while the streamwise noise level measures 91.62 dB, indicating a 14.05 dB lower noise level in the streamwise direction than in the transverse direction.

(3) Based on the results of field experiments and numerical simulations, it has been observed that the actual dominant vibration frequency of 128 Hz closely matches the coupled transverse-longitudinal mode (Mode 4) at 126.82 Hz, as well as the characteristic frequency of bundle aerodynamic noise at 121 Hz. This confirms that the occurrence of acoustic resonance in the heat exchanger is attributed to the excitation of the coupled transverse-longitudinal mode rather than the commonly observed transverse mode. Furthermore, the presence of longitudinal baffles does not effectively suppress the longitudinal mode, thus failing to prevent the onset of acoustic resonance. It is recommended that future revisions of standards take into account such scenarios to mitigate the risk of acoustic resonance.

## Data Availability

The data used to support the findings of this study are available from the corresponding author upon request.

## Conflicts of Interest

The authors declare that they have no conflicts of interest.

## References

[1] D. Fitzpatrick, "A review of cross-flow induced vibrations in heat exchanger tube arrays," *Journal of Fluids and Structures*, vol. 2, 1988.

[2] M. Eid and S. Ziada, "Vortex shedding and acoustic resonance of single and tandem finned cylinders," *Journal of Fluids and Structures*, vol. 27, no. 7, pp. 1035–1048, 2011.

[3] M. Shaaban and A. Mohany, "Characteristics of acoustic resonance excitation by flow around inline cylinders," *Journal of Pressure Vessel Technology*, vol. 141, no. 5, 2019.

[4] O. Afifi and A. Mohany, "Parametric investigation of the flow-sound interaction mechanism for single cylinders in cross-flow," *Journal of Pressure Vessel Technology*, vol. 143, no. 2, 2021.

[5] G. C. Zhou, *Study on Flow-Induced Vibration and Noise Character of Tube Bundles*, Harbin Engineering University, Harbin, China, 2010.

[6] H. Y. Tang, W. K. Jiang, Z. M. Zhong, and Y. J. Zhao, "Research on formation mechanism of low frequency noise in a heat recovery steam generator," *Journal of Chinese Society of Power Engineering*, vol. 34, no. 12, pp. 978–984, 2014.

[7] D. P. Lockard, M. R. Khorrami, M. M. Choudhari, F. V. Hutcheson, T. F. Brooks, and D. J. Stead, "Tandem cylinder noise predictions," in *Proceedings of the AIAA/CEAS Aeroacoustics Conference*, Rome, Italy, May 2007.

[8] G. Q. Liu, *Numerical Investigation on Flow-Induced Noise Around Circular Cylinders at High Reynolds Number*, Huazhong University of Science &Technology, Wuhan, China, 2017.

[9] P. R. Spalart, K. V. Belyaev, M. L. Shur, M. Kh Strelets, and A. K. Travin, "On the differences in noise predictions based on

solid and permeable surface Ffowcs Williams-Hawkings integral solutions," *International Journal of Aeroacoustics*, vol. 18, no. 6-7, pp. 621–646, 2019.

[10] X. Hu, X. Zhang, and Y. You, "On the flow around two circular cylinders in tandem arrangement at high Reynolds numbers," *Ocean Engineering*, vol. 189, Article ID 106301, 2019.

[11] G. Chen, X.-F. Liang, D. Zhou, X.-B. Li, and F.-S. Lien, "Numerical study of flow and noise predictions for tandem cylinders using incompressible improved delayed detached eddy simulation combined with acoustic perturbation equations," *Ocean Engineering*, vol. 224, Article ID 108740, 2021.

[12] Z. Li and J. Li, "Numerical simulation study of aerodynamic noise in high-rise buildings," *Applied Sciences*, vol. 12, no. 19, p. 9446, 2022.

[13] B. Li, X. Xu, J. Wu, L. Zhang, and Z. Wan, "Research on characteristics of flow noise and flow-induced noise," *Applied Sciences*, vol. 13, no. 19, Article ID 11095, 2023.

[14] L. Liu, J. Liu, S. Lyu, S. Lyu, and J. Yin, "Numerical study of a control scheme on flow-induced cavity noise," *Maine Advanced Technology and Engineering Center Web of Conferences*, vol. 283, Article ID 09002, 2019.

[15] K. K. Chode, H. Viswanathan, K. Chow, and H. Reese, "Investigating the aerodynamic drag and noise characteristics of a standard squareback vehicle with inclined side-view mirror configurations using a hybrid computational aeroacoustics (CAA) approach," *Physics of Fluids*, vol. 35, no. 7, 2023.

[16] J. Yangzhou, J. F. Wu, Z. K. Ma, and X. Huang, "Aeroacoustic sources analysis of wake-ingesting propeller noise," *Journal of Fluid Mechanics*, vol. 962, p. A29, 2023.

[17] G. F. Huang, H. Wang, and W. Tan, *Investigation of Acoustic Resonance Phenomenon in a Large-Scale Heat Exchanger, ASME 2023 Pressure Vessels and Piping Conference*, American Society Mechanical Engineers, Atlanta, GA, USA, 2023.

[18] R. B. Langtry and F. R. Menter, "Correlation-based transition modeling for unstructured parallelized computational fluid dynamics codes," *American Institute of Aeronautics and Astronautics Journal*, vol. 47, no. 12, pp. 2894–2906, 2009.

[19] O. Inoue and N. Hatakeyama, "Sound generation by a two-dimensional circular cylinder in a uniform flow," *Journal of Fluid Mechanics*, vol. 471, pp. 285–314, 2002.

[20] K. Ishihara, T. Miyamoto, and Y. Yoshida, "Study on the evaluation of sound speed in ducts with tube banks," *Journal of Environment and Engineering*, vol. 5, no. 2, pp. 339–352, 2010.

[21] D. Tang, S. Bao, B. Lv, H. Cui, L. Luo, and M. Xu, "Investigation of shedding patterns and its influences on lift performances of a cylinder bundle in cross flow," *Journal of Mechanical Science and Technology*, vol. 33, no. 6, pp. 2651–2663, 2019.

[22] M. Weinmann, R. D. Sandberg, and C. Doolan, "Tandem cylinder flow and noise predictions using a hybrid RANS/LES approach," *International Journal of Heat and Fluid Flow*, vol. 50, pp. 263–278, 2014.

[23] C. Read and H. Viswanathan, "An aerodynamic assessment of vehicle-side wall interaction using numerical simulations," *International Journal of Automotive and Mechanical Engineering*, vol. 17, no. 1, pp. 7587–7598, 2020.

[24] C. J. Doolan, "Computational bluff body aerodynamic noise prediction using a statistical approach," *Applied Acoustics*, vol. 71, no. 12, pp. 1194–1203, 2010.

[25] L. N. Jenkins, D. H. Neuhart, C. B. Mcginley, M. M. Choudhari, and M. R. Khorrami, "Measurements of unsteady wake interference between tandem cylinders," in *Proceedings of the 36th AIAA Fluid Dynamics Conference and Exhibit*, Las Vegas, NV, USA, July 2006.

[26] G. A. Brès, D. Freed, M. Wessels, S. Noelting, and F. Pérot, "Flow and noise predictions for the tandem cylinder aeroacoustic benchmark," *Physics of Fluids*, vol. 24, no. 3, 2012.

[27] D. Tang, S. Bao, M. Xu et al., "On the number of tubes required to study oscillating vortices and frequency spectrums of tube arrays in cross flow," *Annals of Nuclear Energy*, vol. 124, pp. 198–210, 2019.